Available online at www.sciencedirect.com
ScienceDirect
International Journal of Heat and Mass Transfer 50 (2007) 967–976
International Journal of HEAT and MASS TRANSFER
www.elsevier.com/locate/ijhmt

Two-dimensional simulation of gas–solid heat transfer in pneumatic conveying

K.S. Rajan [a,*], B. Pitchumani [b], S.N. Srivastava [a], B. Mohanty [c]

[a] School of Chemical and Biotechnology, SASTRA Deemed University, Tirumalaisamudram, Thanjavur 613 402, India
[b] Department of Chemical Engineering, Indian Institute of Technology Delhi, Hauz kaus, New Delhi 110 016, India
[c] Department of Chemical Engineering, Indian Institute of Technology Roorkee, Uttaranchal 247 667, India

Received 8 February 2005
Available online 25 October 2006

Abstract

Gas–solid heat transfer during dilute phase pneumatic conveying is numerically studied by formulating and solving a two-dimensional, two-fluid model. The model is arrived after neglecting minority terms in the governing equations. A new algorithm for solution of governing equations is proposed, that is non-iterative and computationally less intensive. The performance of simulation algorithm is verified in comparison with the literature data. Heat transfer simulations have been carried out for particles of different sizes at a constant solid to gas mass flow ratio. Various aspects of profiles of phase velocities and temperatures and the effect of particle size on these profiles have been discussed.

Keywords: Gas–solid heat transfer; Pneumatic conveying; Model; Simulation algorithm; Particle size

1. Introduction

Pneumatic conveying provides a flexible, convenient and dust free transportation of particulate materials, from one process unit to another in cement, fertilizer, pharmaceutical and other industries [1]. Pneumatic conveying can be classified as dilute phase and dense phase conveying, depending on the state of suspension of particles. In, dilute phase conveying, particles are suspended individually in the gas medium [2] without any interaction between them. High gas velocities are required to achieve dilute phase conveying and a number of applications have been developed based on dilute phase conveying. Dilute phase flow exists in fluid catalytic cracking riser and in circulating fluidized beds. This mode of flow can also be used to design gas–solid heat exchangers and dryers. Batteries of reverse flow cyclones with pneumatic conveying ducts are common in modern cement industries to preheat kiln feed using flue gas. A number of materials like limestone, alumina, iron ore, food and pharmaceutical products are dried using pneumatic dryers. Hydrodynamics of pneumatic conveying in dilute phase has been widely published. Few experimental data is available in the literature for gas–solid heat transfer in pneumatic conveying ducts, where Bandrowski and Kaczmarzyk [3] reported heat transfer from air to ceramic spheres in vertical ducts. Experimental data on pneumatic drying of alumina, limestone, PVC, iron ore, etc., have been published [4–6]. One dimensional, two-fluid models have been developed for simulation of pneumatic drying to predict the temperature profile of gas and the moisture profile of solids [7–9]. Computational analysis of flow structure in dilute phase flow has been reported very widely in the literature, especially in riser of fluid catalytic cracking and circulating fluidized bed units [10–12]. They are confined to simulation of isothermal gas–solid flows. Two-dimensional, two-fluid models for vertical pneumatic dryer have been reported by Skuratovsky in [13,14], and have been verified using one-dimensional

* Corresponding author. Tel.: +91 4362 264101; fax: +91 4362 246120.
E-mail address: rajan_sekar@yahoo.com (K.S. Rajan).

0017-9310/$ - see front matter © 2006 Elsevier Ltd. All rights reserved.
doi:10.1016/j.ijheatmasstransfer.2006.08.009

Nomenclature

A	cross-sectional area of the duct (m^2)
C_d	drag coefficient (–)
C_p	specific heat of gas (J/kg K)
C_{p_s}	specific heat of solid (J/kg K)
D	diameter of duct (m)
D_p	diameter of particle (m)
F_{fg}	frictional force per unit length between gas and the wall (N/m)
F_{fs}	frictional force per unit length between particles and the wall (N/m)
F	fluid–solid interaction forces per unit length (N/m)
f_2	damping function given by Eq. (9)
f_μ	damping function given by Eq. (8)
g	acceleration due to gravity (9.81 m/s^2)
h	convective heat transfer coefficient (W/m^2 K)
h_p	gas–particle heat transfer coefficient (W/m^2 K)
k	turbulent kinetic energy (m^2/s^2)
k_g	thermal conductivity of gas (W/m K)
M	molecular weight of gas
m	mass flow rate (kg/s)
N_s	number of particles per unit volume (m^{-3})
Nu	Nusselt number (–)
Nu_p	Gas-particle Nusselt Number (–)
P	pressure (Pa)
Pr	Prandtl number (–)
Pr_T	turbulent Prandtl number (–)
Q_g	heat transfer rate from gas to solids, per unit length (W/m)
Q_l	rate of heat loss from gas, per unit length (W/m)
Q_s	rate of heat gain by solid from gas, per unit length (W/m)
R	radius of the pipe (m)
Re_p	particle Reynolds number (–)
R_T	turbulent Reynolds number ($=k^2/\gamma\varepsilon$)
r	distance from the centre in the radial direction (m)
S_{g1}	source terms in Eq. (36)
S_{g2}	source terms in Eq. (36)
S_S	source terms in Eq. (37)
T	temperature (K)
U_τ	friction velocity (m/s)
u'	average gas velocity at the inlet (m/s)
u^*	dimensionless gas velocity ($=u(r)/u_c$)
u	velocity (m/s)
u_c	centre-line gas velocity (m/s)
W	work per unit length between the phases (N)
x	distance (m)
y^+	dimensionless distance from the wall ($=[R-r]U_\tau/\gamma$)

Greek symbols

α	thermal diffusivity (m^2/s)
α_T	turbulent thermal diffusivity (m^2/s)
δ	solid volume fraction (–)
ε	rate of dissipation of turbulent kinetic energy (m^2/s^3)
ϕ	variable in Eq. (36)
γ	kinematic viscosity (m^2/s)
γ_T	eddy kinematic viscosity (m^2/s)
μ	viscosity of gas phase (kg/ms)
ρ	gas density (kg/m^3)
ψ	variable in Eq. (37)

Subscripts

g	gas phase
s	solid phase

experimental data. Axial profiles of solid temperature, moisture content, gas temperature, its humidity, etc., at various radial locations in the dryer are presented. All the above methods are based on Semi-Implicit Method for Pressure Linked Equations (SIMPLE) or its modified form, which require guessing of pressure field and then attaining convergence through iterations [15]. In the present work, a modified model and a corresponding solution algorithm are proposed to perform two-dimensional simulation of gas–solid heat transfer in pneumatic conveying. The proposed algorithm is computationally less rigorous.

2. Model

Two-fluid approach is utilized for the modeling of gas–solid heat transfer during pneumatic conveying, in which, both the gas and solid phases are treated as continuum. The following assumptions are made in the model development:

(a) Gas phase is ideal and continuous. The flow is steady and incompressible.
(b) Particle–particle interactions and the contribution of pressure gradient in the solid momentum balance equation are considered to be negligible, as the flow is dilute. Jaberi [16] has shown that the particle collisions are unimportant for dilute flows.
(c) Only momentum and heat interaction between gas and particles and no mass transfer between gas and particles.
(d) The turbulence of the continuous phase is modelled using the k–ε strategies.
(e) Gas phase and solid phase velocities have component in axial direction only and they are functions of the axial and radial location in the pipe.

(f) The momentum contribution due to molecular transport in axial direction in the momentum balance equation is neglected. One-dimensional models reported in the literature have also neglected the momentum contribution in the axial direction, as evident from [7,8]. Also, it has been reported by Skuratovsky et al. [13] that the conductive heat flux in axial direction is negligible in comparison with the convective heat flux. Hence, the conductive flux terms in enthalpy balance equation, turbulent kinetic energy equation and dissipation rate of kinetic energy equation are neglected. This paves way to the development of a fast algorithm for the simulation, as detailed in the subsequent sections.

(g) The effect of particles on the gas phase turbulence has been neglected.

(h) Gas–wall friction, solid–wall friction and heat loss in the conveying duct have been taken into account.

(i) Heat transfer between wall and particles, electrical forces, surface tension forces, Saffman lift forces, Magnus forces and capillary forces are neglected.

3. Model equations

3.1. Gas phase

Continuity equation:

$$\frac{\partial(\rho_g A_g u_g)}{\partial x} = 0 \tag{1}$$

Momentum balance equation:

$$\frac{\partial(m_g u_g)}{\partial x} + A_g \frac{dP}{dx} = -F_{fg} + F_g - A_g \rho_g g + \frac{1}{r}\frac{\partial}{\partial r}\left(r A_g \rho_g (\gamma + \gamma_T)\frac{\partial u_g}{\partial r}\right) \tag{2}$$

Energy balance equation:

$$\frac{\partial(m_g C_p T_g + 0.5 m_g u_g^2)}{\partial x} = Q_g - Q_l - W_g - m_g g + \frac{1}{r}\frac{\partial}{\partial r}\left(r C_p \rho_g A_g (\alpha + \alpha_T)\frac{\partial T_g}{\partial r}\right) \tag{3}$$

Turbulent kinetic energy equation:

$$\frac{\partial(m_g k)}{\partial x} = \rho_g A_g \varepsilon + \frac{1}{r}\frac{\partial}{\partial r}\left(r\rho_g A_g\left(\gamma + \frac{\gamma_T}{1.4}\right)\frac{\partial k}{\partial r}\right) - A_g \rho_g \gamma_T \left(\frac{\partial u_g}{\partial r}\right)^2 \tag{4}$$

Dissipation rate of turbulent kinetic energy equation:

$$\frac{\partial(m_g \varepsilon)}{\partial x} = \frac{f_2 c_1 \rho_g A_g \varepsilon^2}{k} - \frac{c_2 A_g \rho_g \gamma_T \varepsilon}{k}\left(\frac{\partial u_g}{\partial r}\right)^2 + \frac{1}{r}\frac{\partial}{\partial r}\left(r\rho_g A_g\left(\gamma + \frac{\gamma_T}{1.3}\right)\frac{\partial \varepsilon}{\partial r}\right) \tag{5}$$

3.2. Solid phase

Momentum balance equation:

$$\frac{\partial(m_s u_s)}{\partial x} = -F_{fs} + F_s + A_s \rho_s g \tag{6}$$

Energy balance equation:

$$\frac{\partial(m_s C_{p_s} T_s + 0.5 m_s u_s^2)}{\partial x} = Q_s - W_s - m_s g \tag{7}$$

3.3. Eddy viscosity and damping functions

The conventional k–ε equations cannot be integrated up to the wall or in the low Reynolds number region. Two approaches are widely followed to overcome this problem: Wall function method, that bridges the turbulent region with the solid boundary and the low Reynolds number models that make use of empirical damping functions and enable integration up to the wall. The low Reynolds number model of Myong and Kasagi [17] has been found good to predict pipe flow data [18]. Hence, the model of Myong and Kasagi [17] is used in the present study.

The eddy viscosity (γ_T) is defined as

$$\gamma_T = \frac{0.09 f_\mu k^2}{\varepsilon} \tag{8}$$

The empirical functions f_μ and f_2 [in Eq. (5)] are given by

$$f_\mu = \left[1 - \exp\left(\frac{-y^+}{70}\right)\right]\left[1 + \frac{3.45}{\sqrt{R_T}}\right] \tag{9}$$

$$f_2 = \left[1 - \frac{2}{9}\exp\left(\frac{-R_T^2}{36}\right)\right]\left[1 - \exp\left(\frac{-y^+}{5}\right)\right]^2 \tag{10}$$

The turbulent thermal diffusivity (α_T) is the product of turbulent Prandtl number and the eddy viscosity.

4. Complimentary equations

A number of complimentary equations are required for solution of the governing partial differential equations. The total cross sectional area of the pipe is sum of areas occupied by the gas and solid phases

$$A = A_g + A_s \tag{11}$$

The mass flow rate of solid is related to its density, velocity and A_s by,

$$m_s = u_s A_s \rho_s \tag{12}$$

The gas–wall friction has been modeled using the well-known Blasius equation. For modeling particle–wall friction, the equation of Konno and Saito [19] was used.

$$F_{fs} = 0.057\left(m_s\sqrt{\frac{g}{D}}\right) \tag{13}$$

$$Re_p = \frac{\rho_g (u_g - u_s) D_p}{\mu_g} \tag{14}$$

The force of interaction between gas and particle phase is the drag force. Hence,

$$F_s = -F_g = \frac{3C_d A_s \rho_g A^{0.65}(u_g - u_s)^2}{4D_p A_g^{0.65}} \quad (15)$$

The above equation incorporates gas–solid drag coefficient C_d and the expression for drag force which are modified to take into account of multi-particle effects [2]. Drag coefficient was estimated using empirical correlations given in [2].

Work interaction between the gas and particles were modeled as the products of force of interaction and the particle phase velocity.

$$W_g = -W_s = F_g u_s = F_s u_s \quad (16)$$

Non-isothermal pneumatic conveying involves heat transfer between the suspended particles and the gas. The rate of gas–particle heat transfer per unit height is given as

$$-Q_g = Q_s = N_s A \pi D_p^2 h (T_g - T_s) \quad (17)$$

N_s is number of particles per unit volume of the duct, given by

$$N_s = \frac{6A_s}{A\pi D_p^3} \quad (18)$$

The heat transfer coefficient, h_p for the gas–particle heat transfer was determined from the gas–particle Nusselt number, evaluated using Ranz–Marshall equation.

Ranz–Marshall equation:

$$Nu_p = 2 + 0.60(Re_p^{0.5})Pr^{0.33} \quad (19)$$

In the above equation, Pr is the Prandtl number given by

$$Pr = \frac{C_S \mu_g}{k_g} \quad (20)$$

Heat loss in conveying duct per unit height is given by

$$Q_l = \pi D h (T_g - T_w) \quad (21)$$

The convective heat transfer coefficient, h is determined from Nusselt number, determined using the following equation:

$$Nu = 0.023 Re^{0.8} Pr^{0.3} \quad (22)$$

5. Inlet and boundary conditions

The solution of Eqs. (1)–(7) requires boundary conditions to be specified. The symmetry prevailing at the axis requires following boundary conditions at centerline:

$$\frac{\partial u_g}{\partial x} = 0; \quad \frac{\partial T_g}{\partial x} = 0; \quad \frac{\partial k}{\partial x} = 0; \quad \frac{\partial \varepsilon}{\partial x} = 0 \quad (23)$$

Zero value boundary conditions are imposed at the wall for variables u_g, u_s, k. Wall boundary condition for ε is fixed as given in [18]. Temperatures of gas and solid phases are set at the inlet and at wall.

The velocity profile at the inlet, applicable for turbulent flows is given by [15]

$$u_g(r) = 1.2245u'\left(1 - \frac{r}{R}\right)^{\frac{1}{7}} \quad (24)$$

A turbulent intensity of 5% is imposed to calculate the profile of turbulent kinetic energy at the inlet. The dissipation rate of kinetic energy at inlet is calculated using the following formula [15]:

$$\varepsilon(r) = 0.1k(r)\left(1.2245u'\left[1 - \frac{r}{R}\right]^{\frac{-6}{7}}\right)\frac{1}{7R} \quad (25)$$

This results in a steady and fully-developed profile for the gas flow at the inlet. Solid velocity at the inlet is taken as a small fraction of the gas velocity.

6. Simulation algorithm

Solution of gas phase momentum balance equation needs the guessing or evaluation of pressure gradient. Semi-Implicit Method for Pressure Linked Equations (SIMPLE) and many alternatives based on that method have been widely used for solution of gas phase momentum equation, by guessing the pressure gradient and attaining convergence through iteration. It is a computationally laborious process. In the present method, one-dimensional equations are solved from which information on cross-sectional average velocity; solid phase concentration and pressure are obtained. The one-dimensional governing equations can deduced from Eqs. (1)–(7) by neglecting the terms containing derivative with respect to radial position. Turbulent kinetic energy and its rate of dissipation equations need not be solved for one-dimensional simulations in view of assumption (g). The pressure gradient in the one-dimensional gas phase momentum balance equation can be rewritten as described below:

Rewriting Eq. (1)

$$\frac{\partial(\rho_g A_g u_g)}{\partial x} = \frac{\partial\left(\frac{PMA_g u_g}{RT_g}\right)}{\partial x} = \frac{\partial\left(PA_g u_g / T_g\right)}{\partial x} = 0 \quad (26)$$

Applying first-order forward differences to the above equation gives,

$$(PA_g u_g / T_g)_{i+1} = (PA_g u_g / T_g)_i \quad (27)$$

Rewriting the above equation,

$$P_{i+1} = P_i \frac{(A_g u_g)_i (T_g)_{i+1}}{(A_g u_g)_{i+1}(T_g)_i}; \quad (28)$$

Hence,

$$\frac{\partial P}{\partial x} = \frac{P_{i+1} - P_i}{\Delta x} = \frac{P_i}{\Delta x}\left(\frac{(A_g u_g)_i (T_g)_{i+1}}{(A_g u_g)_{i+1}(T_g)_i} - 1\right) \quad (29)$$

Substituting Eq. (29) in one-dimensional gas phase momentum balance equation leaves three unknown u_g, T_g, A_g. Solid phase momentum balance equation is solved to determine solid phase velocity (u_s) and A_s estimated

using Eq. (12). A_g is determined using Eq. (11) from A_s. Simultaneous solution of gas phase momentum and energy balance equations gives gas temperature (T_g) and gas velocity (u_g). Gas pressure is then determined using Eq. (28). The ability of this solution method to predict pressure drop in pneumatic conveying has been illustrated by the corresponding author [20]. Pressure profiles obtained through one-dimensional simulation is used to determine the pressure gradient, for two-dimensional simulations. This can be justified as pressure gradient is independent of radial position in vertical pneumatic conveying. Eqs. (1)–(7) are solved using forward difference scheme for 'x' and central difference scheme for 'r'.

Writing two-dimensional gas phase momentum balance equation in terms of finite differences

$$\begin{aligned}&\frac{(m_g u_g)_{i+1,j}-(m_g u_g)_{i,j}}{\Delta x}+A_{g,i}\frac{P_{i+1}-P_i}{\Delta x}\\&\quad=-F_{fg(i,j)}+F_{g(i,j)}+A_{g(i,j)}\rho_{g(i,j)}g\\&\qquad+\frac{1}{(\Delta r)^2}r_j\left((rA_g\rho_g(\gamma+\gamma_T))_{(i,j+0.5)}\{u_{g(i,j+1)}-u_{g(i,j)}\}\right)\\&\qquad-\frac{1}{(\Delta r)^2}r_j\left((rA_g\rho_g(\gamma+\gamma_T))_{(i,j-0.5)}\{u_{g(i,j)}-u_{g(i,j-1)}\}\right)\end{aligned}\tag{30}$$

While solving the above equation, P_{i+1} and P_i are obtained from results of one-dimensional model, leaving only gas phase velocity as unknown at the axial location $i+1$.

Similarly for gas phase energy balance equation

$$\begin{aligned}&\frac{(m_g C_p T_g+0.5m_g u_g^2)_{i+1,j}-(m_g C_p T_g+0.5m_g u_g^2)_{i,j}}{\Delta x}\\&\quad=Q_{g(i,j)}-Q_{l(i,j)}-W_{g(i,j)}-m_g g\\&\qquad+\frac{1}{(\Delta r)^2}r_j\left((rA_g c_{pg}\rho_g(\alpha+\alpha_T))_{(i,j+0.5)}\{T_{g(i,j+1)}-T_{g(i,j)}\}\right)\\&\qquad-\frac{1}{(\Delta r)^2}r_j\left((rA_g\rho_g c_{pg}(\alpha+\alpha_T))_{(i,j-0.5)}\{T_{g(i,j)}-T_{g(i,j-1)}\}\right)\end{aligned}\tag{31}$$

Gas phase turbulent kinetic-energy equation becomes

$$\begin{aligned}&m_g\frac{(k)_{i+1,j}-(k)_{i,j}}{\Delta x}\\&\quad=\rho_{g(i,j)}A_{g(i,j)}\varepsilon_{(i,j)}-A_{g(i,j)}\rho_{g(i,j)}\gamma_{T(i,j)}\left(\frac{u_{g(i,j+1)}-u_{g(i,j)}}{\Delta r}\right)^2\\&\qquad+\frac{1}{(\Delta r)^2}r_j\left(\left(rA_g\rho_g\left(\gamma+\frac{\gamma_T}{1.4}\right)\right)_{(i,j+0.5)}\{k_{(i,j+1)}-k_{(i,j)}\}\right)\\&\qquad-\frac{1}{(\Delta r)^2}r_j\left(\left(rA_g\rho_g\left(\gamma+\frac{\gamma_T}{1.4}\right)\right)_{(i,j-0.5)}\{k_{(i,j)}-k_{(i,j-1)}\}\right)\end{aligned}\tag{32}$$

Gas phase dissipation rate of turbulent kinetic energy equation becomes

$$\begin{aligned}&\frac{(m_g\varepsilon)_{i+1,j}-(m_g\varepsilon)_{i,j}}{\Delta x}\\&\quad=\frac{f_2c_1\rho_{g(i,j)}A_{g(i,j)}\varepsilon_{(i,j)}^2}{k}-\frac{c_2A_{g(i,j)}\rho_{g(i,j)}\gamma_{T(i,j)}\varepsilon_{(i,j)}}{k_{(i,j)}}\left(\frac{u_{g(i,j+1)}-u_{g(i,j)}}{\Delta r}\right)^2\\&\qquad+\frac{1}{(\Delta r)^2}r_j\left(\left(rA_g\rho_g\left(\gamma+\frac{\gamma_T}{1.3}\right)\right)_{(i,j+0.5)}\{\varepsilon_{(i,j+1)}-\varepsilon_{(i,j)}\}\right)\\&\qquad-\frac{1}{(\Delta r)^2}r_j\left(\left(rA_g\rho_g\left(\gamma+\frac{\gamma_T}{1.3}\right)\right)_{(i,j-0.5)}\{\varepsilon_{(i,j)}-\varepsilon_{(i,j-1)}\}\right)\end{aligned}\tag{33}$$

Solid phase momentum balance equation becomes

$$\frac{(m_s u_s)_{i+1,j}-(m_s u_s)_{i,j}}{\Delta x}=-F_{fs}+F_{s(i,j)}+A_{s(i,j)}\rho_{s(i,j)}g\tag{34}$$

Solid phase energy balance equation becomes

$$\begin{aligned}&\frac{(m_s C_{p_s}T_s+0.5m_s u_s^2)_{i+1,j}-(m_s C_{p_s}T_s+0.5m_s u_s^2)_{i,j}}{\Delta x}\\&\quad=Q_{s(i,j)}-W_{s(i,j)}-m_s g\end{aligned}\tag{35}$$

For the gas phase, the general equation for the variable 'ϕ' can be written as

$$\phi_{(i,j)}=\phi_{(i-1,j)}+\Delta x(S_{g1})+\frac{\Delta x}{(\Delta r)^2}(S_{g2})\tag{36}$$

The variable 'ϕ' can be u_g, T_g, k, ε. S_{g1} and S_{g2} represent source terms in gas phase governing equations that do not, and that containing a derivative in radial direction respectively.

Similarly, for solid phase, the general equation for variable 'ψ' can be written as

$$\psi_{(i,j)}=\psi_{(i-1,j)}+\Delta x(S_S)\tag{37}$$

The variable 'ψ' can be u_s or T_s.

To ensure stability of the proposed method, the ratio $\Delta x/(\Delta r)^2$ must be maintained at a lower value. Decreasing the increment in axial direction, while increasing interval in radial direction would ensure stability and prevent numerically induced oscillations observed with improper choice of grid size. However, increasing interval in radial direction would lend the mesh coarser, leading to poor resolution. Hence, it is advisable to use lower values of increments in axial and radial directions and still maintain a low enough value of the ratio $\Delta x/(\Delta r)^2$, to render the method stable. In the present study, grid sizes in the axial and radial directions are 0.001 and 0.0011, respectively, leading to 2000×14 grids for computations, and the simulations were stable without any numerically induced oscillations and physically unrealistic values. This procedure does not need any iteration and hence computational load is reduced considerably. A typical simulation experiment

consumes approximately 55 s of a P-IV, 128 MB RAM, 1.9 GHz CPU time.

7. Results and discussion

To establish the ability of proposed solution algorithm, simulations were performed to predict the data of Tsuji et al. reported in [21]. The density, pipe diameter, average inlet gas velocity are 1020 kg/m^3, 30 mm and 11.3 m/s respectively. Height of the simulated tube is 2 m. Simulations were carried out for same gas and solid inlet temperatures and at the solid to gas mass flow ratios of 0.6, 2 and 3 for 1 mm particles and at the solid to gas mass flow ratios of 1.3 and 1.9 for 0.2 mm particles to simulate data of Tsuji et al. In order to compare the simulated data with the data of Tsuji et al., radial profiles of simulated dimensionless gas velocity (ratio of actual gas velocity to centre-line gas velocity) are plotted in Figs. 1 and 2 for all the simulated cases. The experimental data of Tsuji et al. are also shown for the sake of comparison. It is clear from Figs. 1 and 2 that the simulated results agree reasonably well with the data of Tsuji et al. It can also be seen that the introduction of solids has smoothened the velocity profiles at all solid to gas mass flow ratios. Deviations from the experimental data near the wall may be due to assumptions of negligible particle–particle interaction and gas phase turbulence modulation, since solid concentrations near the wall are higher in dilute phase flows. Having demonstrated the ability of proposed algorithm to predict the flow profile, simulations are performed for gas–solid heat transfer in pneumatic conveying by using different values for solid and gas inlet temperatures.

7.1. Effect of particle size

Simulations were performed for heat transfer between cold particles at 293 K and hot air at 493 K. The particle density, duct diameter, solid to gas mass flow ratio are 1020 kg/m^3, 30 mm and 2 respectively. The particle diameters simulated are 2, 1, 0.5 and 0.2 mm. At the wall,

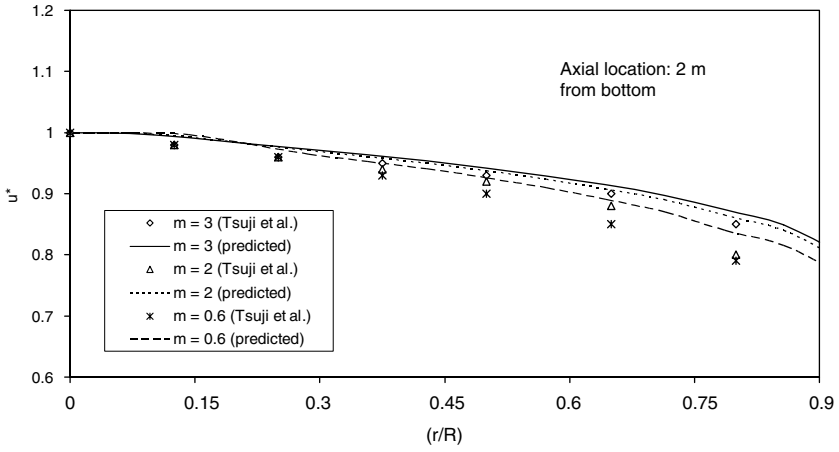

Fig. 1. Simulated and experimental profiles of dimensionless gas phase velocity at different radial positions, while conveying 1 mm particles at different solid to gas mass flow ratios.

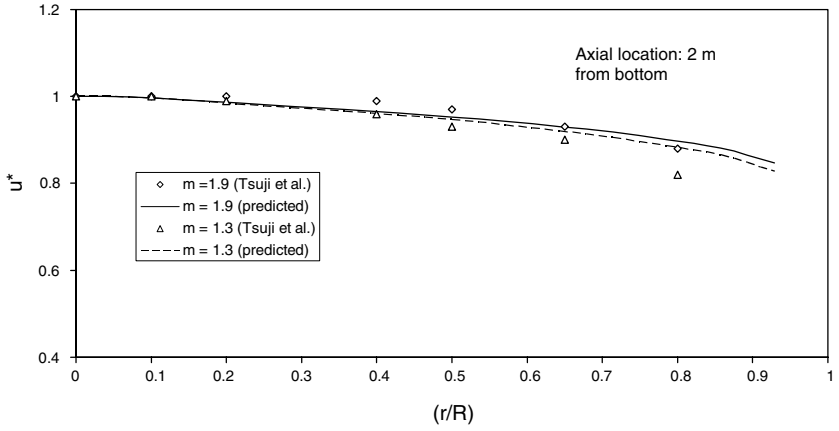

Fig. 2. Simulated and experimental profiles of dimensionless gas phase velocity at different radial positions, while conveying 0.2 mm particles at different solid to gas mass flow ratios.

gas temperature is obtained by solving the following equation [22]:

$$-k\frac{dT_g}{dr} = h(T_g - T_w) \tag{38}$$

Specifying boundary condition for solid temperature at the wall in non-isothermal flow is difficult with this simplified model and simulation method. Hence, the solid temperature at the wall is taken to be closer to solid temperature at the neighboring grid. Fig. 3 shows the radial profiles of gas velocity at a height of 2 m from the inlet, while conveying these particles. It can be inferred from Fig. 3 that, at a height of 2 m from the bottom of the duct, gas velocities at all points in a cross section are higher with larger particles and decrease with decrease in particle size. The reasons for this behavior are described below.

Pressure drop for conveying of particles is mainly due to the drag between gas and solids. For a fixed solid to gas mass flow ratio, with increase in particle size, the drag force between the solids and gas decreases and hence the pressure drop also decreases, leading to higher absolute pressure along the height of the duct and this is evident from Fig. 4, where a plot of variation of pressure with height is made for different particle sizes. But, with larger particles, the rate of heat transfer is less owing to lower surface area per unit volume of the duct, resulting in higher gas temperature, compared to while conveying smaller particles. This high temperature leads to high gas velocity despite high absolute pressure, while conveying large cold particles. If gas and solid were initially at same temperature, lower gas velocities would have been observed with large particles.

Fig. 5 shows the radial profile of dimensionless gas velocity while conveying particles of 2 mm, 1 mm, 0.5 mm and 0.2 mm at a solid to gas mass flow ratio of 2, with the initial gas temperature of 493 K and solid temperature

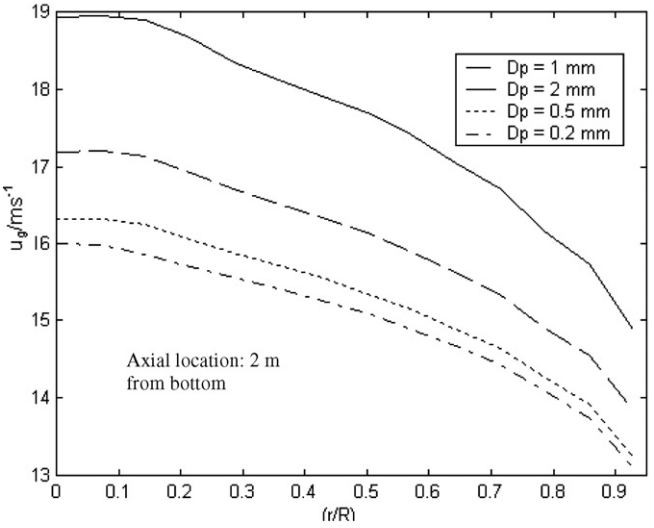

Fig. 3. Simulated radial profiles of gas velocity while conveying cold particles of different sizes at a solid to gas mass ratio of 2.

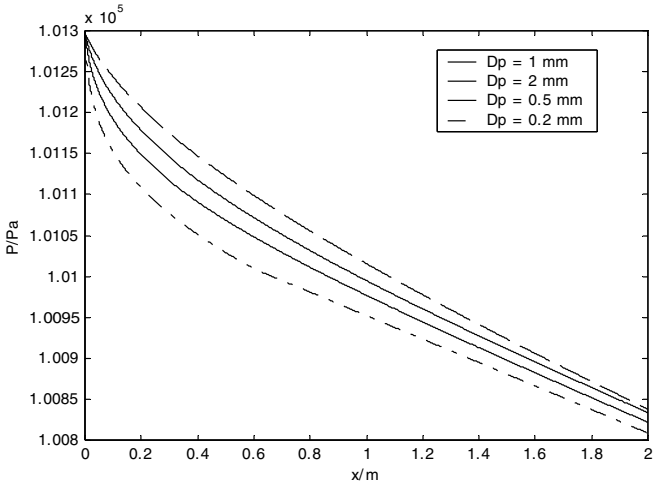

Fig. 4. Variation of gas pressure with axial position in the conveying duct for conveying cold particles of different sizes at a solid to gas mass ratio of 2.

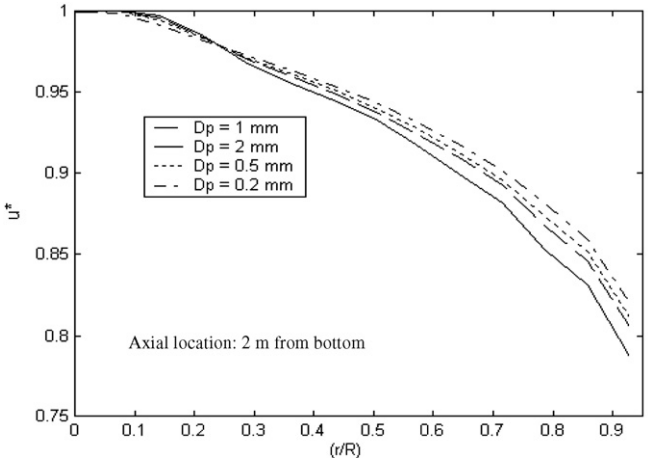

Fig. 5. Simulated radial profiles of dimensionless gas velocity, while conveying particles of different sizes at a solid to gas mass ratio of 2.

of 293 K. It can be observed from Fig. 5, that the trend of dimensionless gas velocity profiles for different particle sizes has changed at a location 25% away from the axis. From the axis till 25% away from it, dimensionless gas velocity increases with increase in particle size, while at locations towards the wall, dimensionless gas velocity decreases with increase in particle size. This phenomenon can be understood by studying the nature of source terms in radial direction in the gas momentum balance equation. At locations near the wall, solid concentrations and relative velocity would be high, resulting in reduced gas velocities at these locations due to larger drag. Hence the dimensionless gas velocity is less near the wall. This is especially severe for large particles. For smaller particles, the gas velocity profile (as seen from Fig. 3) is more uniform, resulting in relatively higher dimensionless gas velocity near the wall. Moving away from the wall, the gas velocity profiles become flatter for all particle sizes and hence at a

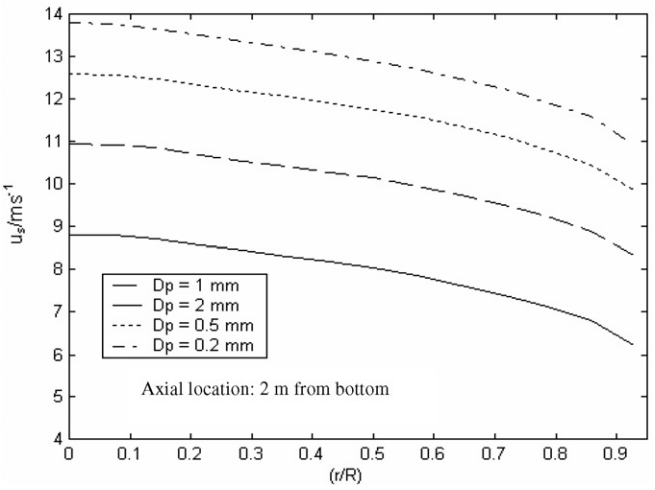

Fig. 6. Simulated radial profiles of solid phase velocity for particles of different sizes at a solid to gas mass ratio of 2.

point near 25% from the axis, the dimensionless velocities with all the particle sizes are same. Near the axis, solid concentrations with larger particles are less than that with small particles and hence the gas velocity profile is more uniform while conveying large particles than the smaller particles. This results in higher dimensionless gas velocities with large particles near the axis.

Fig. 6 shows the variation of solid velocity in the radial direction for the particle sizes under study for a solid to gas mass flow ratio of 2 with initial gas and solid temperatures being 493 K and 293 K, respectively. Since, no turbulence or collision model has been used for the solid phase in the simulations, trends of solid velocity profiles match with that of gas velocity profiles, for all the particle sizes.

The plot of solid volume concentrations at various radial positions is needed to infer important features of gas velocity and temperature profiles. Hence such a plot is drawn in Fig. 7. It can be seen from Fig. 7, that for all the particles sizes, the solid concentrations are minimum near the axis and increase to a maximum towards the wall. Also, with large particles, higher solid volume concentrations are achieved due to slower acceleration, than that with smaller particles. Also, it is worthy to note that the profiles of solid volume concentration are more uniform with smaller particles, than with larger particles, especially near the wall, signifying possibility of important differences in their behavior in dynamics and heat transfer. Though, the maximum average solid concentration obtained in this study is greater than 0.001, the flow may be taken to be dilute, due to lower solid to gas mass flow ratio and accordingly the effect of particle–particle collision can be neglected with little error.

Fig. 8 shows the plot of variation of gas temperature in the radial direction for the particle sizes under study for a solid to gas mass flow ratio of 2, with the initial gas and solid temperatures being 493 K and 293 K. It can be seen from Fig. 8, that the profiles of solid volume concentration and gas velocity affect profile of gas temperature. In the developing region or in the initial portions of the duct, near the wall, high solid concentrations prevail, and hence higher heat transfer area, leading to higher heat removal from gas, despite lower gas velocity. Hence, lower gas temperature is observed near the wall. The height of this region depends on the particle size for a fixed solid to gas mass flow ratio. After this height, the rate of heat transfer near the axis would be more, compared to that at the wall, due to high gas velocity at the axis and more uniform distribution of solid concentration across the cross-section. Since the simulations have been performed at a height of 2 m, larger particles would be still in the initial height, while for particles of 0.5 mm and 0.2 mm, the heat transfer

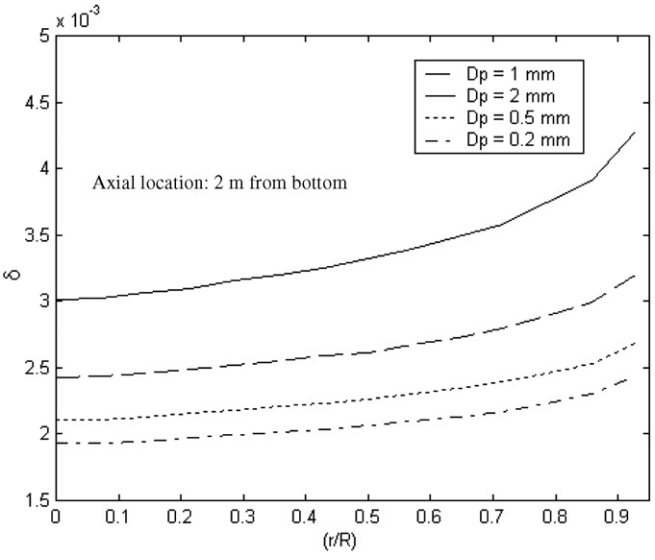

Fig. 7. Solid volume concentrations at various radial locations, for particles of different sizes at the solid to gas mass ratio of 2.

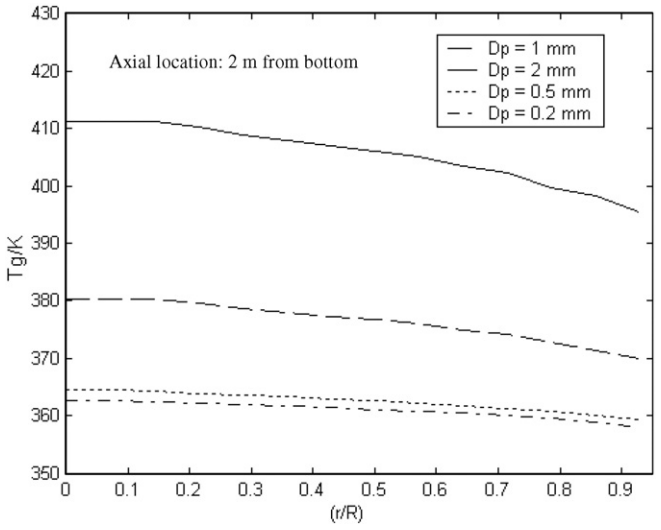

Fig. 8. Variation of gas temperature with radial position, for particles of different sizes.

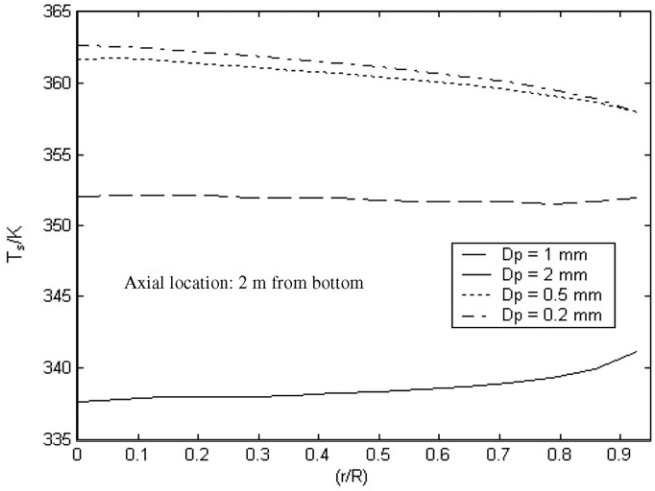

Fig. 9. Variation of solid temperature with radial position, for particles of different sizes.

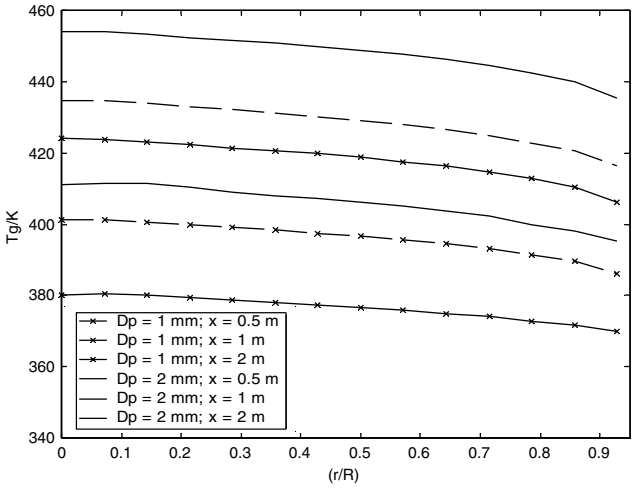

Fig. 10. Simulated radial profiles of gas temperature at different heights, while conveying particles of 1 mm and 2 mm diameter.

rates are uniform leading to lower gradient in temperature profiles.

Fig. 9 shows the plot of profile of solid temperature in the radial direction for the particle sizes under study at a solid to gas mass flow ratio of 2, with the initial gas and solid temperatures being 493 K and 293 K, respectively. It can be seen from Fig. 9, that the solid temperature increases from the centre towards the wall for particles of 2 mm size. For such a large particle, as described previously, at this height high heat transfer rates will be achieved near the wall. Hence, the temperature of solids are high near the wall, when compared to that at the centre, where solid concentrations and hence heat removed from the gas are low. But, for particles of size 0.5 mm and 0.2 mm, it is evident from Fig. 9 that the solid temperature is maximum at centre and is lower at the wall. For such smaller particles, the source term in solid phase energy balance equation are high at the axis than that at the wall and hence, solids at the axis gain more heat than that at the wall and hence higher temperature are achieved near the axis, while the reverse holds good for 2 mm particles. In this study, for the conditions examined, for 1 mm particles, the solid temperature profile is nearly flat indicating that a transition is expected at this height for 1 mm particles.

The developing nature of the flow can be visualized by comparing the temperature profiles for particles of different sizes at three heights of 0.5, 1 and 2 m. Such plots are made in Figs. 10 and 11. Fig. 10 shows radial profiles of gas temperature while conveying particles of 2 mm and 1 mm size. Lines with marker correspond to the profiles of gas temperature while conveying 1 mm particles and the lines without marker indicate the profiles while conveying 2 mm particles. It is evident from Fig. 9 that the flow is thermally developing, as there is change in gas temperature at different heights. Also, the profiles at different heights are similar. For 1 mm particles, though the flow is not fully

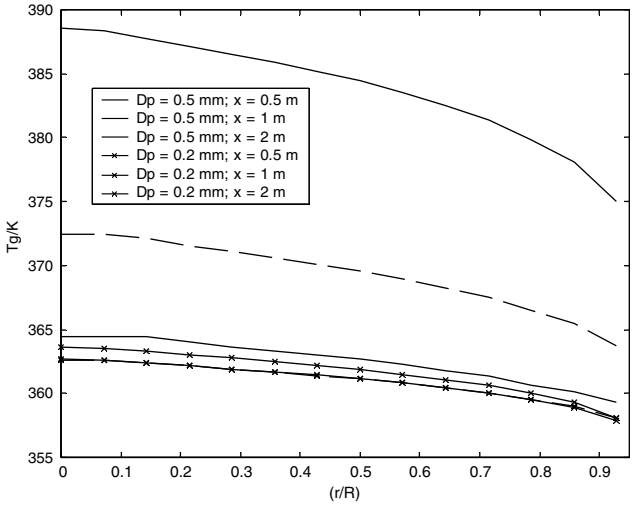

Fig. 11. Simulated radial profiles of gas temperature at different heights, while conveying particles of 0.2 mm and 0.5 mm diameter.

thermally developed, the gas temperature profile at a height of 2 m is more uniform compared to profiles at the heights of 0.5 and 1 m. Similar plots are made in Fig. 11 for particles of size 0.2 and 0.5 mm. It can be observed from Fig. 11, that for particles of 0.2 mm, the flow is fully developed at the height of 1 m, as the profiles of gas temperature at heights of 1 and 2 m overlap. This shows that for smaller particles, due to high heat transfer rates, much of the heat transfer is accomplished over a smaller height of the duct. In other words, flow is fully developed at a smaller height and excess height of the duct provided would only increase pressure drop and hence the power consumption. Plots of solid temperature profiles at heights of 0.5, 1 and 2 m are also shown in Figs. 12 and 13 for different particles sizes simulated.

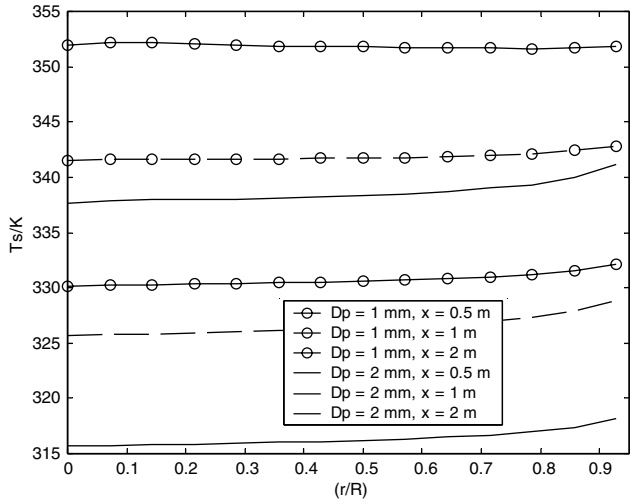

Fig. 12. Simulated radial profiles of solid temperature at different heights, while conveying particles of 1 mm and 2 mm diameter.

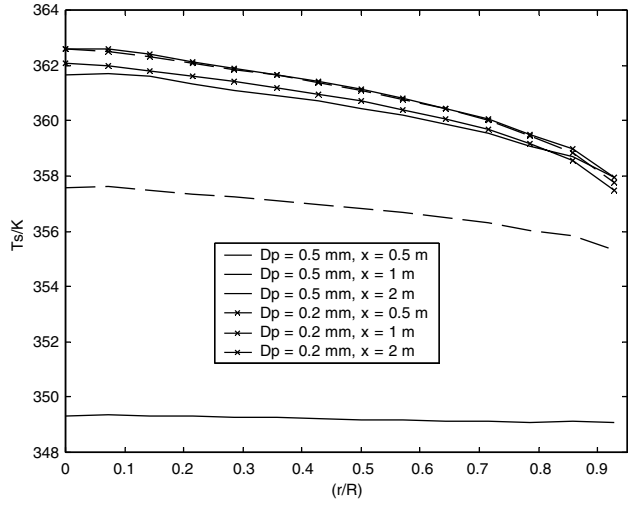

Fig. 13. Simulated radial profiles of solid temperature at different heights, while conveying particles of 0.5 mm and 0.2 mm diameter.

8. Conclusions

The proposed two-dimensional, two-fluid model and a new, fast simulation algorithm predict the literature data reasonably well for dilute phase flow simulations. Deviations of predictions from literature data may due to the negligence of particle–particle collisions and turbulence modulation by particles. The model predicts the dynamics and heat transfer in dilute gas–solid vertical flow very well. Profiles of gas and solid phase velocities and temperatures for different size particles show the effect of particle size on flow behavior and heat transfer. These simulations help to understand the gas–solid heat transfer phenomenon and can serve as a tool for further parametric studies.

References

[1] O. Molerus, Overview: pneumatic transport of solids, Powder Technol. 88 (1996) 309–321.
[2] A. Levy, Two-fluid approach for plug flow simulations in horizontal pneumatic conveying, Powder Technol. 112 (2000) 263–272.
[3] J. Bandrowski, G. Kaczmarzyk, Gas-to-particle heat transfer in vertical pneumatic conveying of granular materials, Chem. Eng. Sci. 33 (1976) 1303–1310.
[4] R.D. Radford, A model of particulate drying in pneumatic conveying systems, Powder Technol. 93 (1997) 109–126.
[5] J. Baeyens, D. Van Gauwbergen, I. Vinckier, Pneumatic drying: the use of large-scale experimental data in a design procedure, Powder Technol. 83 (1995) 139–148.
[6] Won Namkung, Minyoung Cho, Pneumatic drying of iron ore particles in a vertical tube, Drying Technol. 22 (2004) 877–891.
[7] Avi Levy, David J. Mason, David Levi-Hevroni, Irene Borde, Drying of wet particles in a steady-state one-dimensional flow, Powder Technol 95 (1998) 15–23.
[8] Avi Levy, Irene Borde, Steady state one dimensional flow model for a pneumatic dryer, Chem. Eng. Process. 38 (1999) 121–130.
[9] A.H. Pelegrina, G.H. Crapiste, Modelling the pneumatic drying of food particles, J. Food Eng. 48 (2001) 301–310.
[10] G. Ferschneider, P. Mège, Dilute gas–solid flow in a riser, Chem. Eng. J. 87 (2002) 41–48.
[11] Lu Huilin, Dimitri Gidaspow, Jacques Bouillard, Liu Wentie, Hydrodynamic simulation of gas–solid flow in a riser using kinetic theory of granular flow, Chem. Eng. J. 95 (2003) 1–13.
[12] Haosheng Zhou, G. Flamant, D. Gauthier, Jidong Lu, Lagrangian approach for simulating the gas–particle flow structure in a circulating fluidized bed riser, Int. J. Multiphase Flow 28 (2002) 1801–1821.
[13] I. Skuratovsky, A. Levy, I. Borde, Two-fluid, two-dimensional model for pneumatic drying, Drying Technol. 1 (2003) 1645–1668.
[14] I. Skuratovsky, A. Levy, I. Borde, Two-dimensional numerical simulations of the pneumatic drying in vertical pipes, Chem. Eng. Process. 44 (2005) 187–192.
[15] A.K. Das, J. De Wilde, G.H. Heynderickx, G.B. Marin, J. Vierendeels, E. Dick, CFD simulation of dilute phase gas–solid reactors: Part I – a new solution method and flow model validation, Chem. Eng. Sci. 59 (2004) 167–186.
[16] F.A. Jaberi, Temperature fluctuations in particle-laden homogenous turbulent flows, Int. J. Heat Mass Transfer 41 (1998) 4081–4093.
[17] H.K. Myong, N. Kasagi, A new approach to the improvement of k–ε turbulence model for wall-bounded shear flows, JSME Int. J. (Series II) 33 (1990) 63–72.
[18] C.M. Hrenya, E.J. Bolio, D. Chakrabarti, J.L. Sinclair, Comparison of low Reynolds number k–ε turbulence models in predicting fully developed pipe flow, Chem. Eng. Sci. 50 (12) (1995) 1923–1941.
[19] H. Konno, S.J. Saito, Pneumatic conveying of solids through straight pipes, Japanese Chem. Eng. 2 (1969) 211–217.
[20] Rajan KS, Ponnusai V, Srivastava SN. Modelling and simulation of gas–particle flow in dilute phase pneumatic conveying using finite difference technique. In: Bora SN. (editor), Proceedings of the international conference on environmental fluid mechanics, Guwahati; 2005. p. 236–43.
[21] Y. Tsuji, Turbulence in gas–solid flows, in: N.P. Cheremisninoff (Ed.), Encyclopedia of fluid mechanics, Gulf Publishing, Houston, 1986, pp. 9.299–9.301.
[22] Mercado ERL, Souza VC, Guirardello R, Nunhez JR. Modeling flow and heat transfer in tubes using a fast CFD formulation, Comput. Chem. Eng. 25;2001:713–22.